Magnetocrystalline anisotropy of Laves phase $Fe_2Ta_{1-x}W_x$ from first principles: Effect of 3*d*-5*d* hybridization

Alexander Edström
Department of Physics and Astronomy, Uppsala University, Box 516, 75121 Uppsala, Sweden
and Materials Theory, ETH Zürich, Wolfgang-Pauli-Strasse 27, 8093 Zürich, Switzerland
(Received 20 December 2016; revised manuscript received 1 June 2017; published 17 August 2017)

The magnetic properties of Fe_2Ta and Fe_2W in the hexagonal Laves phase are computed using density functional theory in the generalized gradient approximation, with the full potential linearized augmented plane-wave method. The alloy $Fe_2Ta_{1-x}W_x$ is studied using the virtual crystal approximation to treat disorder, with some comparisons to supercell calculations. Fe_2Ta is found to be ferromagnetic with a saturation magnetization of $\mu_0 M_s = 0.66$ T while, in contrast to earlier computational work, Fe_2W is found to be ferrimagnetic with $\mu_0 M_s = 0.35$ T. The transition from the ferri- to the ferromagnetic state occurs for $x \leqslant 0.1$. The magnetocrystalline anisotropy energy (MAE) is calculated to 1.25 MJ/m^3 for Fe_2Ta and 0.87 MJ/m^3 for Fe_2W. The MAE is found to be smaller for all values x in $Fe_2Ta_{1-x}W_x$ than for the end compounds and it is negative (in-plane anisotropy) for $0.1 \leqslant x \leqslant 0.9$. The MAE is carefully analyzed in terms of the electronic structure. Even though there are weak 5*d* contributions to the density of states at the Fermi energy in both end compounds, a reciprocal space analysis, using the magnetic force theorem, reveals that the MAE originates mainly from regions of the Brillouin zone with strong 3*d*-5*d* hybridization near the Fermi energy. Perturbation theory and its applicability in relation to the MAE is discussed.

DOI: 10.1103/PhysRevB.96.064422

I. INTRODUCTION

The magnetocrystalline anisotropy energy (MAE) is the intrinsic relativistic feature, originating from spin-orbit coupling (SOC) [1], of magnetic materials that the energy depends on the direction of magnetization relative to the crystal lattice. It is crucial in a wide range of applications, from permanent magnets [2–5] to magnetic storage devices [6]. The SOC is strong in heavy elements such as rare earths (REs) and actinides which consequently acquire large MAE, while in applications it is highly desirable to obtain a large MAE without such expensive or inaccessible constituent elements [7]. One compound which has gained much attention due to its huge MAE is tetragonal FePt [8–12]. This material acquires its magnetization mainly from Fe, while the important factors resulting in the large MAE include the strong SOC of the Pt atom, as well as the uniaxial crystal structure. The crystal structure is crucial because highly symmetric, e.g., cubic, crystals tend to have at least one order of magnitude lower MAE. Nevertheless, FePt contains large amounts of the valuable element Pt, whereby alternative magnetic 3*d*-5*d* composites in uniaxial crystal structures can be of great technological value. One such compound is hexagonal Laves phase (C14) Fe_2W, which was reported by Arnfelt and Westgren [13] and recently attracted some attention in the context of permanent magnet replacement materials [14,15]. Early electronic structure calculations [16] failed to establish the existence of ferromagnetism in the compound from the Stoner criterion. While it now seems clear that the compound is magnetically ordered [14,15], a thorough understanding of the magnetism in this material appears to be absent in the literature and some discrepancies can be seen between recent computational [14] and experimental work [15]. For example, calculations [14] overestimated the saturation magnetization by nearly 30% and provided a vastly different MAE when compared to experimental data from nanoparticles [15]. It is therefore the purpose of this work to use state-of-the-art electronic structure calculations to unambiguously determine the magnetic ground state of the Fe_2W compound and investigate the magnetic properties, including the technologically important intrinsic properties of saturation magnetization (M_s) and MAE. The closely related compound Fe_2Ta is isostructural to Fe_2W [17] and also studied. Some focus will be put on the MAE, which will be carefully analyzed in terms of the electronic structure. Furthermore, the possibility to tune the MAE by alloying W and Ta will be examined and a discussion of the underlying physical principles provided.

II. COMPUTATIONAL METHODS

Density functional theory (DFT) calculations in the generalized gradient approximation [18] (GGA) were performed with the full-potential linearized augmented plane waves (FP-LAPW) method as implemented in WIEN2K [19]. Initially, spin-polarized calculations were performed in the scalar relativistic approximation, but to calculate the MAE, SOC must be included and this was done in a second variational approach [20]. The size of the basis set used is typically described by the product of the smallest muffin-tin sphere and the largest reciprocal-lattice vector included, $RK_{\max}$. For structure optimizations, this value was set to $RK_{\max} = 7$, while for MAE calculations a larger value of $RK_{\max} = 9$ was used. To obtain a well converged formation energy, a value as large as $RK_{\max} = 9.5$ was needed. Integration of **k** points over the Brillouin zone was performed using the improved tetrahedron method [21] and 700 **k** points in the full Brillouin zone (48 in the irreducible wedge of the Brillouin zone after considering the 24 symmetry operations of the crystal) were used for structure optimization, 1500 for the calculation of formation energy, and as many as 30 000 **k** points were used in order to obtain well converged MAE values.

III. RESULTS: Fe_2Ta AND Fe_2W

One unit cell of the relevant crystal structure contains two inequivalent Fe positions with multiplicity 2 and 6 respectively,

TABLE I. Lattice parameters and parameters of the internal atomic positions, magnetic moments, saturation magnetization, and formation energy of Fe2W and Fe2Ta as calculated in a scalar relativistic, spin polarized GGA calculation, neglecting SOC, in WIEN2K.

	Fe_2Ta	Fe_2W
a (Å)	4.811	4.674
c (Å)	7.874	7.768
x_{Fe_2}	0.83192	0.82946
z_{5d}	0.06405	0.06924
$m(Fe_1)(\mu_B)$	0.90	−1.14
$m(Fe_2)(\mu_B)$	1.43	1.17
$m(5d)(\mu_B)$	−0.24	−0.05
$m_{tot}(\mu_B/\text{u.c.})$	8.88	4.45
$\mu_0 M_s$ (T)	0.66	0.35
Formation energy (eV/u.c.)	−2.82	−0.63

as well as two equivalent 5*d* sites. Calculations were performed with the initial spin state either in ferro- or ferrimagnetic configurations, i.e., parallel or antiparallel alignment of spins on the two different Fe positions. In the case of Fe_2Ta, the total energy was found to be 7.9 meV per unit cell lower in the case of ferromagnetic ordering compared to ferrimagnetic ordering. For Fe_2W, on the other hand, all calculations converged into the ferrimagnetic state, regardless of initial spin configuration and lattice parameters. This indicates that there is a change of sign in the sum over exchange interactions between Fe_1 and Fe_1 sites when exchanging Ta for W. The magnitude of this change could be estimated by comparing the energy differences for parallel and antiparallel spin arrangements. However, since the Fe_2W calculations converge to the antiparallel spin configuration regardless of the initial spin configuration, this is not possible with the currently used methods. Instead a more detailed analysis of the exchange interactions could be performed using more suitable methods, such as that of Liechtenstein *et al.* [22]. This would require introducing different computational methods and is considered beyond the scope of the current work.

Lattice parameters were calculated by minimizing the total energy with respect to volume and c/a and relaxing the internal atomic positions in each step. The calculated lattice parameters are reported in Table I, which also contains spin magnetic moments and the corresponding saturation magnetizations as well as formation energies. For Fe_2Ta, the lattice parameters have been experimentally reported as $a = 4.833$ Å and $c = 7.868$ Å [17] and for Fe_2W, $a = 4.727$ Å and $c = 7.704$ Å [13], in close agreement with the calculated values in Table I, although for Fe_2W, c/a is slightly larger in the calculated data. The Fe moments in Fe_2W are of similar size and opposite sign but as there are two and six of the respective Fe sites in one unit cell, there is a net total of $4.45\mu_B$/u.c., corresponding to a saturation magnetization of $\mu_0 M_s = 0.35$ T. Since in Fe_2Ta the Fe moments are parallel, the total magnetic moment and corresponding saturation magnetization is significantly larger, reaching a value of $\mu_0 M_s = 0.66$ T. Ta and W have small induced moments of $-0.24\mu_B$ and $-0.05\mu_B$, antiparallel to the total magnetic moment, respectively, as is typical for these 5*d* atoms in a magnetic 3*d* host [23].

Since a different magnetic ordering, with a magnetic moment close to zero on the first Fe site and a larger moment moment around $1.3\mu_B$ on the second Fe atom, has been reported in earlier computational work (pseudopotential DFT calculations in the GGA) [14] for Fe_2W, further investigation seems necessary to unambiguously determine the correct magnetic ground state within the GGA. Hence, fixed spin moment calculations, allowing the total magnetic moment of the system to be constrained to a fixed given value, were performed. The total magnetic moment was varied around the value of $6.8\mu_B$/u.c., previously reported [14]. Magnetic moments of $-0.05\mu_B$ and $1.25\mu_B$ were then obtained on the two Fe atoms, which is similar to the earlier computational results [14]. Initially, the lattice parameters were set to the values mentioned in Ref. [14], but then attempts were made at optimizing the crystal structure with fixed magnetic moment to lower the energy further. However, all calculations resulted in total energies which were higher than those obtained for the structure given in Table I and no minimum could be located in the total energy as a function of total magnetic moment. Based on these results, the most probable conclusion appears to be that the authors of Ref. [14] assumed a ferromagnetic order as initial state and reached a local energy minimum for which the magnetic moments were reported. The correct magnetic moments corresponding to the global energy minimum, within the GGA, based on all results obtained here, are expected to be those in Table I. The explanation given here is consistent with the observation that the previous computational work presented a value of $\mu_0 M_s$ as approximately 0.56 T which overestimated the experimental low-temperature value of approximately $\mu_0 M_s = 0.44$ T. Nevertheless, the value given in this work somewhat underestimates the experimental result. A possible source of discrepancy is surface effects of the nanoparticles, where enhanced magnetic moments could appear near the surface.

Somewhat surprisingly, a non-negligible difference is seen also in lattice parameters and total magnetic moment for Fe_2Ta, when comparing to previous computational work [14], where $a = 4.825$ Å and $c/a = 1.6329$ (corresponding to $c = 7.879$ Å) was reported. The difference in a is merely 2% and might be expected for the two different computational methods. The difference in total spin magnetic moment is, however, larger. For example, the magnetic moment on the Fe_1 is computed to $0.90\mu_B$, while the other authors reported a value well above $1\mu_B$. The reason for this discrepancy is difficult to pinpoint exactly, as both sets of calculations are performed in the GGA [18], but might partly be related to the difference in lattice parameters.

By comparing the total energy of Fe_2(Ta/W) in the calculated ground state with that of bcc Fe and bcc Ta or W, the formation energy was calculated to −0.63 eV/u.c. for Fe_2W, which is lower than the value close to zero previously reported [14]. A negative formation energy is expected for a stable phase and a possible scenario appears to be that the authors of Ref. [14] obtained a too high formation energy due to calculating a local energy minimum and thus a too high total energy. For Fe_2Ta, the formation energy is lower and this compound may therefore be expected to be more stable and form more easily in nature.

TABLE II. Spin magnetic moments m_S, orbital magnetic moments m_L, saturation magnetizations, and MAE for Fe_2W as calculated in WIEN2K, including SOC with magnetization either along 100 or 001 directions and using the lattice parameters presented in Table I.

Fe_2Ta	**m**∥100	**m**∥001
$m_S(Fe_1)(\mu_B)$	0.943	0.932
$m_S(Fe_2)(\mu_B)$	1.433	1.432
$m_S(Fe_3)(\mu_B)$	1.427	1.432
$m_S(Ta)(\mu_B)$	−0.240	−0.238
$m_L(Fe_1)(\mu_B)$	0.070	0.109
$m_L(Fe_2)(\mu_B)$	0.091	0.099
$m_L(Fe_3)(\mu_B)$	0.101	0.099
$m_L(Ta)(\mu_B)$	0.033	0.034
$\mu_0 M_s$ (T)	0.69	0.69
Energy (meV/u.c.)	1.24	0
Energy (MJ/m^3)	1.25	0
Fe_2W	**m**∥100	**m**∥001
$m_S(Fe_1)(\mu_B)$	−1.148	−1.150
$m_S(Fe_2)(\mu_B)$	1.163	1.172
$m_S(Fe_3)(\mu_B)$	1.172	1.172
$m_S(W)(\mu_B)$	−0.044	−0.044
$m_L(Fe_1)(\mu_B)$	−0.066	−0.151
$m_L(Fe_2)(\mu_B)$	0.045	0.039
$m_L(Fe_3)(\mu_B)$	0.074	0.039
$m_L(W)(\mu_B)$	0.002	0.002
$\mu_0 M_s$ (T)	0.36	0.35
Energy (meV/u.c.)	0.79	0
Energy (MJ/m^3)	0.87	0

In order to compute the MAE, calculations were performed including SOC, which also results in a nonzero orbital magnetic moment, that is otherwise quenched. The computed spin magnetic moments (m_S), orbital magnetic moments (m_L), and MAEs are listed in Table II. When the magnetization is along the a axis, the SOC results in a lowering of symmetry so that the second Fe site with initially six equivalent atoms are split into two types with two and four Fe atoms of each, labeled Fe_2 and Fe_3 respectively. Hence, the spin and orbital moments are the same for Fe_2 and Fe_3 when the magnetization is along the c axis but not when it is along the a axis. The MAE is calculated to $E_{MAE} = 1.24$ meV/u.c. $= 1.25$ MJ/m^3 for Fe_2Ta and $E_{MAE} = 0.79$ meV/u.c. $= 0.87$ MJ/m^3 for Fe_2W, with easy magnetization axis along the c direction of the crystal in both cases. The calculated uniaxial MAE for Fe_2W presented here is in better agreement with the small uniaxial MAE recently presented in experimental work [15] than the large in plane MAE previously computed for the Fe_2W compound [14]. Nevertheless, the computed value found in this work is significantly larger than the reported experimental value of 286 kerg/cm^3 $=$ 28.6 kJ/m^3. However, measurements have only been presented for nanoparticles, while unambiguous MAE measurements require single crystals. For Fe_2Ta, an experimental MAE has not been found in the literature, but the value calculated here differs notably from the value of $E_{MAE} = -1.4$ meV/u.c. previously calculated [14]. This discrepancy is most likely related to the difference in magnetic moments obtained, as mentioned above, but could also be partially related to other computational details, such as the treatment of SOC or core electrons.

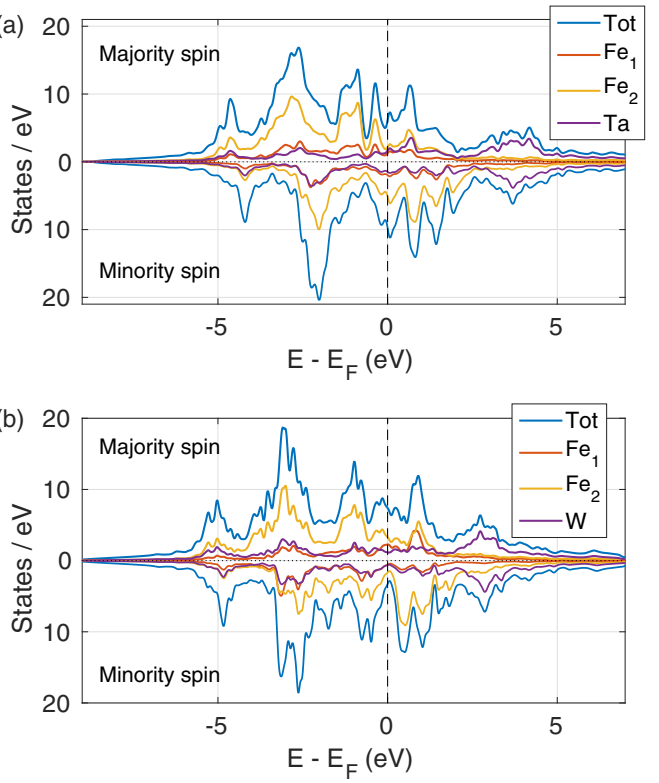

FIG. 1. Spin polarized DOS for Fe_2Ta in (a) and Fe_2W in (b).

Figure 1 shows the spin polarized density of states (DOS) for Fe_2Ta (a) and Fe_2W (b). The majority spin DOS is similar for the two compounds, with the Fermi energy (E_F) at approximately the same location. However, as Ta is exchanged for W more electrons are added into the system and the minority spin states become occupied, whereby these are shifted more to the left in Fig. 1(b) and, as a result, E_F coincides with the bottom of a valley in the minority spin DOS of Fe_2W. Thus the DOS(E_F) for Fe_2W is dominated by minority spin states, in contrast to Fe_2Ta, where the opposite is true. This fact will be of importance later when analyzing the relation between MAE and orbital moment anisotropy. It is also interesting to note that the minority spin DOS of Fe_2W has a valley at E_F, resulting in a higher degree of spin polarization of the DOS(E_F) compared to Fe_2Ta. In both cases, the DOS(E_F) is dominated by Fe, with rather modest contributions from the 5d atoms. This might be one important reason, together with other details in the band structure around E_F, why these compounds do not possess larger MAE. Even the $L1_0$ phase of MnAl exhibits an MAE well above 1 MJ/m^3 [24] without any constituent element heavier than a 3d atom. Heavier atoms, such as 5d's, should allow significantly larger MAE, e.g., 4 MJ/m^3 [10] or more [25] in FePt. However, this requires significant 3d-5d hybridization around E_F, as is seen in FePt [26], but appears to be limited in the compounds studied here. Nevertheless, the contribution from Ta (3.2 states/eV for both spin channels summed) is greater than that of W (1.8 states/eV). This is consistent with the observation that the MAE is greater in the compound containing Ta, although

other differences in the electronic structure are also expected to play a role.

In a system with weak SOC, such as 3*d*-based itinerant magnets, where ξ is significantly smaller than the bandwidth (less than 100 meV compared to several eV), it is reasonable to describe the effect of SOC in terms of perturbation theory and important insights can be gained by doing so [27–29]. For a uniaxial crystal the leading term is of second order while for cubic crystals it is fourth order. Andersson *et al.* [29] discussed the case of having several atomic types and hybridization between these in a tight-binding description. One can consider unperturbed single-particle states at the point $\mathbf{k}$ in the Brillouin zone as

$$|\mathbf{k},i\rangle = \sum_{q,\mu} c_{\mathbf{k},i,q,\mu}\,|\mathbf{k},q,\mu,\sigma_i\rangle\,, \tag{1}$$

with summation over atomic sites q and orbital states μ, but not over the spin σ_n since the unperturbed states each have well defined spin. With on-site SOC, The shift in the energy eigenvalue $E_{\mathbf{k},i}$ associated with $|\mathbf{k},i\rangle$ is

$$\Delta E_{\mathbf{k},i}(\hat{\mathbf{n}}) = -\sum_{j\neq i}\sum_{qq'}\sum_{\mu\mu'\mu''\mu'''} n_{\mathbf{k},i,q\mu,q'\mu'''} n_{\mathbf{k},j,q'\mu'',q\mu'} \cdot \frac{\langle q\mu\sigma_i|\xi_q\hat{\mathbf{l}}\cdot\hat{\mathbf{s}}|q\mu'\sigma_j\rangle\langle q'\mu''\sigma_j|\xi_{q'}\hat{\mathbf{l}}\cdot\hat{\mathbf{s}}|q'\mu'''\sigma_i\rangle}{E_{\mathbf{k},j}-E_{\mathbf{k},i}}, \tag{2}$$

with occupation numbers $n_{\mathbf{k},i,q\mu,q'\mu'''} = c^*_{\mathbf{k},i,q,\mu}c_{\mathbf{k},i,q',\mu'''}$ and spin and orbital angular momentum operators $\hat{\mathbf{s}}$ and $\hat{\mathbf{l}}$. For a given q and $\mathbf{k}$, it is clear that the effect of the SOC is determined by matrix elements of the form $\langle\mu_i,\sigma_i|\,\hat{\mathbf{l}}\cdot\hat{\mathbf{s}}\,|\mu_j,\sigma_j\rangle$ and for convenience these are listed with respect to spin and d orbitals in the Appendix. $\hat{\mathbf{n}}$ is the spin quantization axis (magnetization direction) and the dependence of $\Delta E_{\mathbf{k},i}(\hat{\mathbf{n}})$ on this quantity comes from the SOC matrix elements. For the total shift in $E_{\mathbf{k},i}$, the coupling between all states $j\neq i$ should be considered. However, if both i and j denote occupied states there will be a cancellation when these are summed over to compute the total energy. Therefore, only coupling between occupied and unoccupied states are relevant, except possibly in the small regions of the Brillouin zone where deformations of the Fermi surface occur, as was pointed out by Kondorskii and Straube [27]. This leads to the important and well established conclusion that the MAE is determined by the electronic band structure near the Fermi energy, in particular by the coupling between occupied and unoccupied states [27,30,31]. One more important observation from Eq. (2) is that regions in the band structure with significant Fe-Ta hybridization will allow MAE contributions of order $\frac{\xi_{\mathrm{Ta}}\xi_{\mathrm{Fe}}}{E_{\mathbf{k},j}-E_{\mathbf{k},i}}$, which is significantly larger than $\frac{\xi^2_{\mathrm{Fe}}}{E_{\mathbf{k},j}-E_{\mathbf{k},i}}$, since ξ_{Ta} is several times larger than ξ_{Fe}, or similarly for W instead of Ta.

The discussion above is motivation to perform a careful analysis of the electronic band structure near the Fermi energy to obtain a better understanding of the MAE. Figures 2(a)–2(f) show the spin polarized band structure through various high-symmetry points in the Brillouin zone, without SOC, for Fe_2Ta, with spin-up states on the left side and spin-down states on the right side. Color coding is used to show the orbital character of the bands with red, green, and blue indicating $m = 0$ (d_{z^2}), $m = 1$ (d_{xz} or d_{yz}) and $m = 2$ (d_{xy} or $d_{x^2-y^2}$) character, respectively, for different atomic types in the different rows. A black region on a band indicates that the given atomic type is not significantly contributing to the band there. The large number of bands present, even within one electron volt from the Fermi surface, and complicated band structure with further complication due to hybridization, makes analysis of the MAE in terms of the band structure difficult. Some observation can, nevertheless, directly be made. The Γ point is often of particular importance since it has the highest symmetry. Here there are occupied and unoccupied spin-up states very near the Fermi energy at this point, potentially allowing very strong effect from the SOC, especially since these states both show strong Ta contributions and Ta has the largest SOC constant. However, the unoccupied band is largely of $m = 0$ character, while the occupied one is of $m = 1$ character. Such states do not couple via SOC (see Table IV), whereby the potentially strong MAE contribution at Γ is absent.

To obtain information about which regions in reciprocal space are particularly important to the MAE, the band structures after applying SOC with magnetization along either 100 or 001 directions are plotted in Fig. 2(g). From these bands the MAE contribution per $\mathbf{k}$ point can be evaluated using the magnetic force theorem [32], by taking the difference of the sum over occupied energy eigenvalues for different magnetization directions, which is also plotted (red line, right y axis) in Fig. 2(g). To confirm that the force theorem provides an accurate description of the MAE in the relevant materials, the difference between occupied Kohn-Sham eigenvalues for different magnetization directions was also integrated over the Brillouin zone to yield a value for the MAE. This resulted in 1.26 meV/u.c. for Fe_2Ta and 0.76 meV/u.c. for Fe_2W, in excellent agreement with the results from total-energy calculations presented in Table II. Since the MAE is positive in Fe_2Ta, regions with positive MAE contributions are expected to outweigh the negative regions. In agreement with the observation mentioned about Γ above, there is a rather weak MAE contribution from the region around that point. Instead, it is clear that the most important region is that around the A point where a large and positive MAE contribution is seen, while other regions show smaller values of varying sign, which one might expect to nearly cancel out in a Brillouin-zone integration. From a first look at the bands in Figs. 2(a)–2(f), the most important bands for the MAE at A should be the highest occupied and lowest unoccupied ones, which are in both cases spin-down with fourfold degeneracy. However, in Fig. 2(g) one can identify the strongest positive MAE contribution where occupied 001 bands (blue dashed line) are shifted well below the corresponding 100 bands (black dash-dotted line). This occurs mainly for the highest occupied (also fourfold degenerate) spin-up bands at A, whereby these should also be considered. The three sets of band which thus far appear most important at A all have significant contributions from several atomic types and orbitals, in particular Ta and Fe_1, $m = 1$ and $m = 2$ states, but for the lowest unoccupied spin-down bands, Fe_2 $m = 1$ and $m = 2$ are also important. This means that detailed analysis of the MAE contribution from the A point is complicated since a large number of terms from Eq. (2) must be considered. It is clear, however, that there is a significant

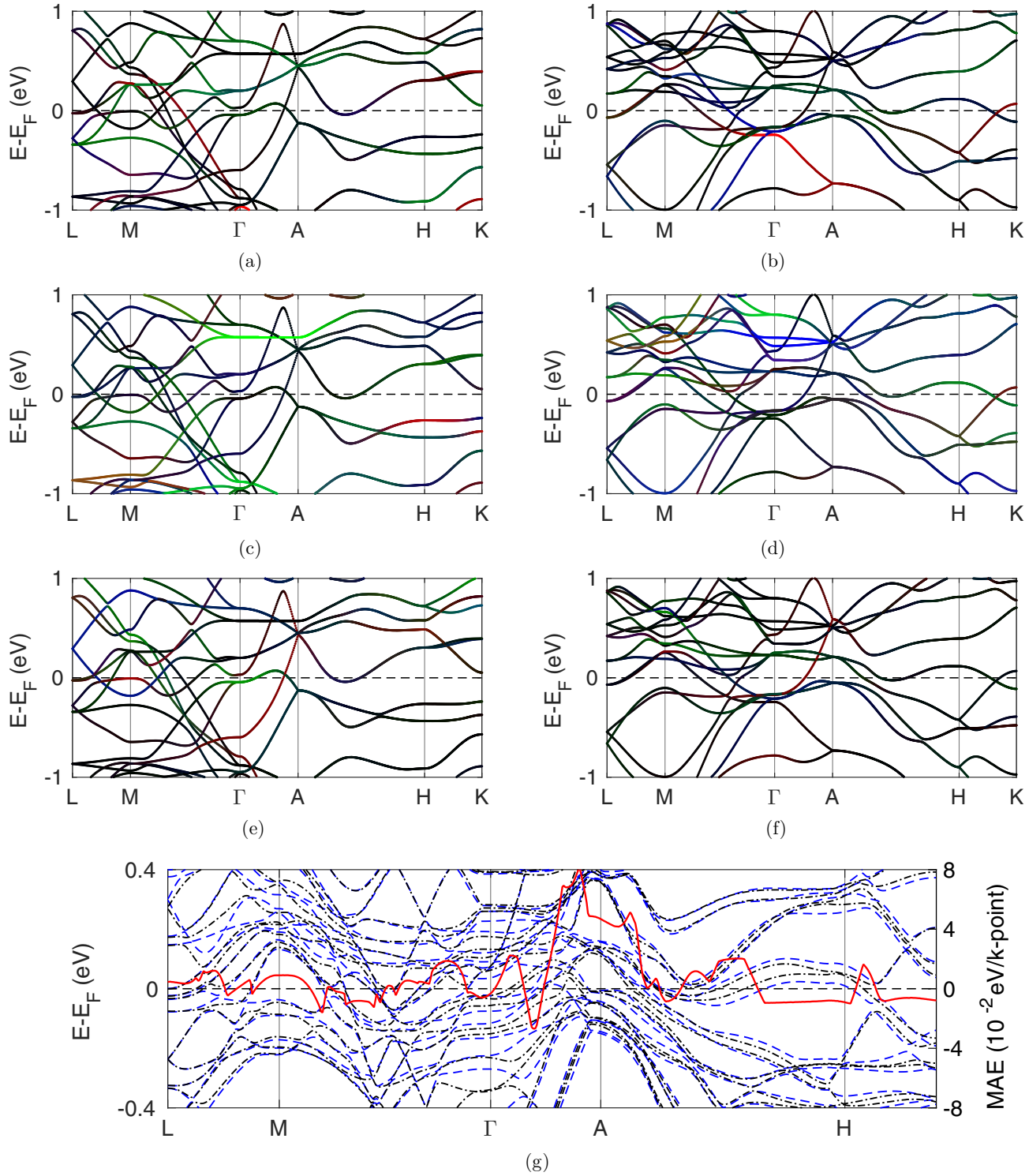

FIG. 2. Atomic type and spin resolved band structure of Fe_2Ta with the colors red, green, and blue indicating the contribution of $m = 0$ (d_{z^2}), $m = 1$ (d_{xz} or d_{yz}) and $m = 2$ (d_{xy} or $d_{x^2-y^2}$) states respectively, in (a)–(f). Black bands indicate that the d orbitals of given atomic type do not contribute significantly to the band in that region. (a) Fe_1, spin up. (b) Fe_1, spin down. (c) Fe_2, spin up. (d) Fe_2, spin down. (e) Ta, spin up. (f) Ta, spin down. (g) Band structure including SOC with magnetization along 100 (black dash-dotted line) or 001 direction (blue dashed line) as well as the MAE contribution per k point (red solid line), obtained via the magnetic force theorem.

Fe-Ta hybridization in the relevant region and as was pointed out above, this allows for significant additions to the MAE.

Figure 3 contains the same type of information as Fig. 2, but for Fe_2W. Since Fe_2W also has a uniaxial (positive) MAE, positive regions are expected to dominate the MAE contributions in Fig. 3(g). In similarity with the Fe_2Ta case, there are large regions of small contributions with varying sign, which one would expect to nearly vanish in an integration. In

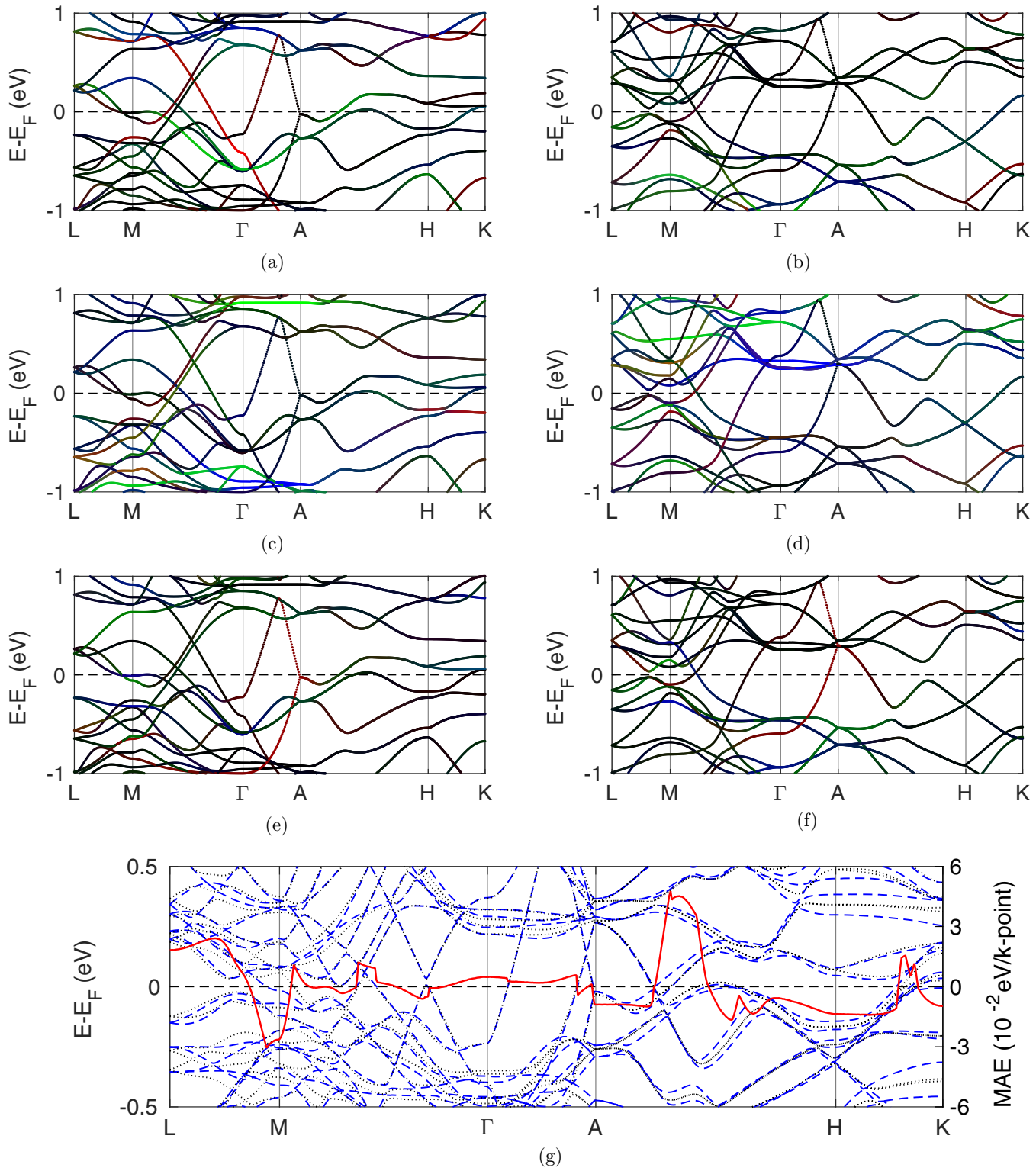

FIG. 3. Atomic type and spin resolved band structure of Fe_2W with the colors red, green, and blue indicating the contribution of $m = 0$ (d_{z^2}), $m = 1$ (d_{xz} or d_{yz}), and $m = 2$ (d_{xy} or $d_{x^2-y^2}$) states respectively, in (a)–(f). Black bands indicate that the d orbitals of given atomic type do not contribute significantly to the band in that region. (a) Fe_1, spin up. (b) Fe_1, spin down. (c) Fe_2, spin up. (d) Fe_2, spin down. (e) W, spin up. (f) W, spin down. (g) Band structure including SOC with magnetization along 100 (black dash-dotted line) or 001 direction (blue dashed line) as well as the MAE contribution per k point (red solid line), obtained via the magnetic force theorem.

particular, the important Γ point provides a weak contribution, which can be understood from the relatively large separation in energy between the highest occupied and lowest unoccupied states, compared to other regions. The most important positive contributions to the MAE stem from the L neighborhood, as well as a region along the path A-H, while there is a significant negative region around M, which can partially explain why the MAE of Fe_2W is not stronger. In the important region along the A-H path, there are two spin-up bands nearly parallel to each other. These are on opposite sides of the Fermi energy where the **k**-point resolved MAE is strongest, and can therefore contribute to the MAE. Both bands are mainly of W and Fe_1 $m = 1$ character. From the SOC matrix elements in the Appendix, one finds that states of same spin and m value yield a positive (uniaxial) contribution to the MAE. Furthermore, the Fe-W hybridization allows the strong W SOC to enhance the coupling strength and this explains the large positive MAE contribution in that part of the A-H path.

At the L point, a significant positive source of MAE is found in the highest occupied spin-up states which are mainly Ta and Fe_1 $m = 1$, since the 001 bands are shifted below the 100 bands. This situation is reversed as one moves along the L-M path and the change of sign in the **k**-resolved MAE appears to coincide with the spin-down bands which are unoccupied at L becoming occupied near M. The presence of many bands with significant hybridization effects makes it difficult to pinpoint states coupling via SOC which are particularly important to the MAE along the L-M path. Nevertheless, it should be pointed out that once again there is significant Fe-W hybridization, so that the strong W SOC can increase the MAE. Since there is a limited 5d contribution to the DOS at the Fermi energy, there can only be significant 3d-5d hybridization near the Fermi energy in a limited region of the Brillouin zone. Nevertheless, the reciprocal space analysis of the electronic structure and MAE contributions reveals that the MAE is mainly determined by those regions in the Brillouin zone where there is notable 3d-5d hybridization, in both Fe_2Ta and Fe_2W.

As both quantities are due to the SOC, Bruno [28] pointed out the close relation between magnetocrystalline anisotropy and orbital moments and showed, using perturbation theory on a tight-binding model, that if deformations of the Fermi surface can be neglected and the MAE is dominated by spin-diagonal coupling, the MAE and orbital magnetic-moment anisotropy are proportional. If coupling between minority spin states dominates the SOC, a maximum orbital magnetic moment is expected in the easy direction of magnetization, as is seen in the case of Fe_2Ta in Table II. If, on the other hand, the SOC is dominated by the coupling between majority spin states, a maximum orbital magnetic moment is expected along the hard magnetization axis, as is seen in the case of Fe_2W. This is consistent with the observation made in Fig. 1 that the Fe_2Ta DOS(E_F) is dominated by minority spin states, while the opposite is true for Fe_2W. For a further analysis of the relation between MAE and m_L in the studied systems, energy and orbital moments have been computed as functions of the angle θ (with $\phi = 0$) when the magnetization is along $\hat{\mathbf{n}} = (\sin\theta\cos\phi, \sin\theta\sin\phi, \cos\theta)$. The result for the energy as function of θ is shown in Fig. 4. The second-order perturbation theory for a uniaxial system leads to the conclusion that the

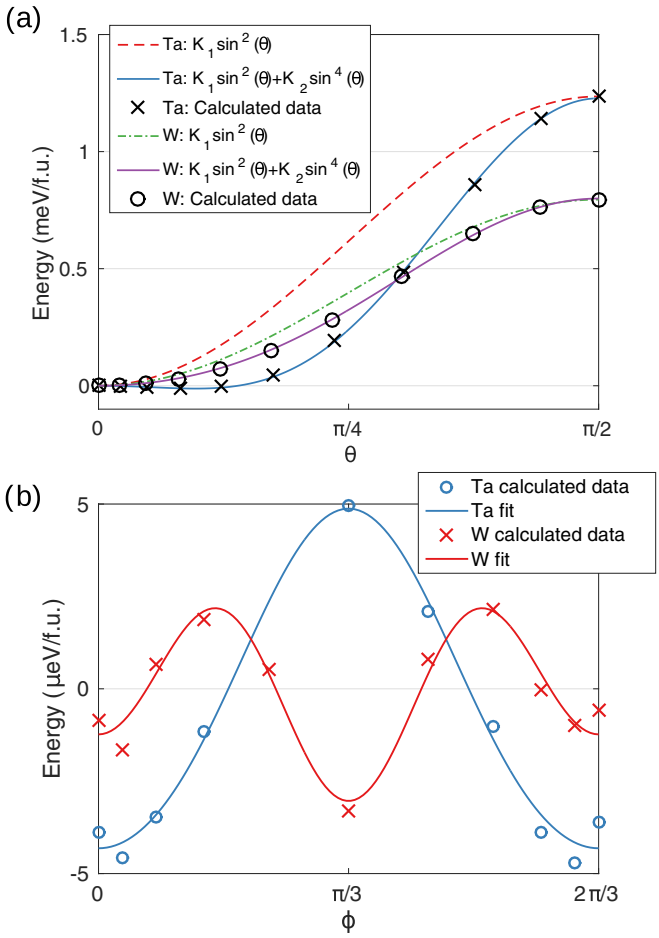

FIG. 4. Energy as a function of the polar angle θ between the c axis and the magnetization direction in (a) and energy as a function of the azimuthal angle ϕ with $\theta = \frac{\pi}{2}$ in (b). The fit in (b) is to a function $E(\theta = \frac{\pi}{2}, \phi) = C_1 + C_2\cos 3\phi + C_3\cos 6\phi$ and $C_2\cos 3\phi + C_3\cos 6\phi$ is plotted.

energy as function of θ follows the relation

$$E(\theta) = K_0 + K_1\sin^2\theta, \tag{3}$$

with isotropic energy K_0. This is merely the first part of the longer expansion

$$E(\theta,\phi) = K_0 + K_1\sin^2\theta + K_2\sin^4\theta + K_3\sin^6\theta \times (1 + k_{3,3}\cos 3\phi + k_{3,6}\cos 6\phi) + \cdots, \tag{4}$$

valid for a uniaxial crystal with threefold rotational symmetry about the z axis, such as the one studied here. For a system where the MAE is well described by second-order perturbation theory, one expects that the energy is well fitted by Eq. (3) and that K_i is vanishingly small for $i > 1$. As seen in Fig. 4(a), fitting the energy as function of angle between magnetization direction and 001 direction to $K_1\sin^2\theta$ provides an unsatisfactory curve for $E(\theta)$ for both Fe_2Ta and Fe_2W, while including also the term $K_2\sin^4\theta$ yields an excellent fit [for the fit to $K_1\sin^2\theta$, K_1 was simply set to $E(\pi/2) - E(0)$, while the fit to $K_1\sin^2\theta + K_2\sin^4\theta$ was done with the method of least squares]. This indicates that second-order perturbation theory provides a quantitatively inaccurate description of the MAE in the studied compounds, while fourth-order terms should provide an accurate description with higher (than

TABLE III. Anisotropy constants K_1, K_2, and $\tilde{K}_3 = K_3(1 + k_{3,3} + k_{3,6})$ from least-squares fitting of $E(\theta,\phi = 0)$ to $K_1 \sin^2\theta + K_2 \sin^4\theta$ or $K_1 \sin^2\theta + K_2 \sin^4\theta + \tilde{K}_3 \sin^6\theta$ (see Fig. 4).

	K_1 (meV/f.u.)	K_2 (meV/f.u.)	$\tilde{K}_3$ (meV/f.u.)
Fe_2Ta	−0.27	1.50	
Fe_2Ta	−0.19	1.23	0.19
Fe_2W	0.50	0.30	
Fe_2W	0.45	0.46	−0.11

fourth)-order corrections being small. Clearly, the fit to $K_1 \sin^2\theta$ is significantly better in the case of Fe_2W than for Fe_2Ta. This indicates that restriction to second-order perturbation theory, rather than fourth, is a better approximation for the W compound, which might be related to the smaller contribution of the $5d$ atom to the DOS(E_F), making the assumption of a small ξ more realistic.

The anisotropy constants obtained from the fitting to $K_1 \sin^2\theta + K_2 \sin^4\theta$ are listed in Table III. As was already anticipated from Fig. 4(a), K_2 is of more importance in Fe_2Ta and in fact it is of opposite sign and significantly bigger than K_1. In the case where K_1 and K_2 have the same sign, the θ derivative of $E(\theta) = K_1 \sin^2\theta + K_2 \sin^4\theta$ has only two zeros for real K_i, namely $\theta = 0$ and $\theta = \pi/2$, whereby the easy and hard magnetization directions will occur at these angles. For opposite signs of K_1 and K_2, an additional zero occurs at

$$\theta = \sin^{-1}\left(\sqrt{-\frac{K_1}{2K_2}}\right) \tag{5}$$

and for Fe_2Ta there is a minimum in the energy at approximately $\theta = 0.15 = 8.8^\circ$. The easy magnetization direction is thus expected at this angle rather than at $\theta = 0$, so the material strictly speaking does not have a uniaxial magnetization. For Fe_2W, both constants are positive so $\theta = 0$ is the easy axis. Although in this case the magnitude of K_1 is greater than K_2, the latter is not negligible.

Table III also contains parameters from a fit to $K_1 \sin^2\theta + K_2 \sin^4\theta + \tilde{K}_3 \sin^6\theta$. This indicates non-negligible values of $\tilde{K}_3$ for both compounds and, in the case of Fe_2Ta, it is of the same magnitude as K_1. However, it is not clear how many fitting parameters are reasonable to include with the given numerical accuracy. Comparison to a fit from a calculation with only 2×10^4 **k** points yields a value smaller by a factor of 1/3 for Fe_2Ta, indicating that the numerical accuracy might be insufficient. However, more accurate calculations become prohibitively computationally demanding.

Typically, in uniaxial systems which do not possess strong SOC, the variation in energy for rotations of the magnetization direction in the plane is small. This makes it challenging and computationally heavy to compute the in-plane magnetic anisotropy (this might differ in, for example, actinide systems, where even cubic materials can have enormous MAE [33]). Nevertheless, the energy as a function of ϕ with $\theta = \frac{\pi}{2}$ was computed and the result is shown in Fig. 4(b). The calculated points have been fitted to $E(\theta = \frac{\pi}{2},\phi) = C_1 + C_2 \cos 3\phi + C_3 \cos 6\phi$ (C_2 and C_3 should correspond to $K_3k_{3,3}$ and $K_3k_{3,6}$, respectively) and C_1 has been subtracted from the calculated points and fitted curves. As expected, the variations in Fig. 4(b)

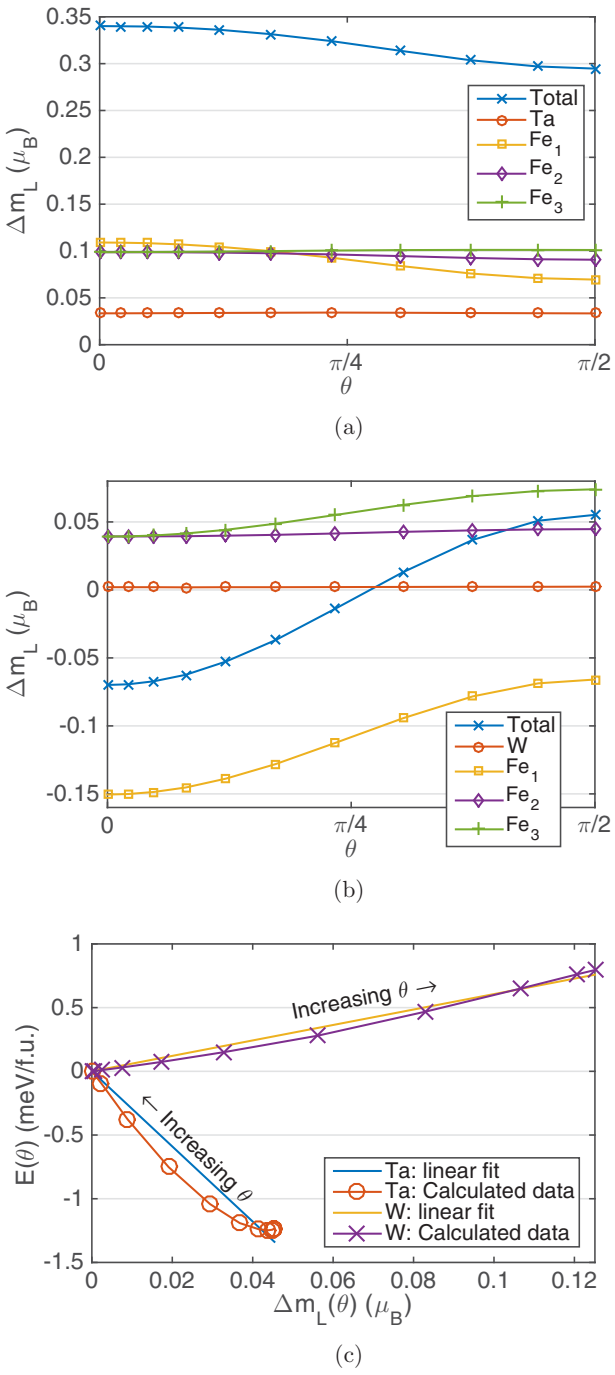

FIG. 5. Energy and orbital magnetic moments as function of the angle θ between the magnetization direction and the 001 axis. (a) Orbital magnetic moment as function of θ for Fe_2Ta. (b) Orbital magnetic moment as function of θ for Fe_2W. (c) Change in energy versus change in orbital moment as θ is varied from 0 to $\pi/2$.

are much smaller, by nearly three orders of magnitude, than the variations seen in Fig. 4(a). It is difficult to say whether the deviations between the computed points and the fitted lines are mainly due to limitations in the numerical accuracy or because of neglecting higher-order terms.

Figure 5 shows how the orbital magnetic moments vary with magnetization direction for Fe_2Ta (a) and Fe_2W (b). In both materials the greatest contribution to the orbital moment

anisotropy is due to the Fe_1 atom. The Fe_2 and Fe_3 atoms have identical orbital magnetic moments at $\theta = 0$, as expected from symmetry, while they deviate from one another at other directions. The compounds differ in the sign of the variation of the orbital magnetic moment with θ, although they both have the same sign of $K_1 + K_2$. In Fig. 5(c), which shows a plot of the energy as function of θ vs the anisotropy in total orbital magnetic moment as function of θ, this appears as a difference in the sign of the slope of the curves. As was previously mentioned, this can be understood in terms of the DOS(E_F) which is mainly due to the majority spin channel in Fe_2W and mainly due to the minority spin channel for Fe_2Ta. According to the work of Bruno [28], this should lead to approximate proportionality between $\Delta m_L(\theta)$ and $E(\theta)$, but with opposite signs in the proportionality constants. However, that was based on second-order perturbation theory, and as was seen above, fourth-order perturbation theory is expected to be necessary for a quantitative description of the magnetic anisotropy in these materials, especially in Fe_2Ta. Figure 5(c) also shows a linear fit to the curves for $E(\theta)$ vs $\Delta m_L(\theta)$. For Fe_2W, the linear fit provides a reasonable description of the curve, while in Fe_2Ta the deviation from linearity is more pronounced. This might largely be because of strong spin polarization of the DOS at E_F for Fe_2W, which makes the approximation that only spin diagonal SOC contributes to the magnetic anisotropy more realistic. Although the DOS(E_F) in Fe_2Ta is dominated by minority spin states, the contribution from the majority spin channel is significant, whereby neglecting spin-off diagonal contributions is questionable. Furthermore, the stronger contribution from the 5*d* states could also affect the relation between MAE and orbital moment anisotropy in that direction, consistent with previous observations [29] of nonproportionality between orbital magnetic moment and anisotropy in energy systems with significant 3*d*-5*d* hybridization.

IV. RESULTS: $Fe_2Ta_{1-x}W_x$

As the MAE depends sensitively on the band structure around the Fermi energy, it can be controlled by tuning the band structure around the Fermi energy. In practice this can be done, for example, by alloying. This will be explored next by considering the alloy $Fe_2Ta_{1-x}W_x$. Reports regarding the stability of the alloy $Fe_2Ta_{1-x}W_x$ appear to be absent in the literature and a thorough investigation into the phase stability is beyond the scope of the current work. However, the existence of both end compounds indicates that it is not unreasonable to expect also the alloy to form for at least some range of x. A computational study of the properties of the alloy indicates whether efforts to synthesize the material is worthwhile and, furthermore, can shed light on similarities and differences between Fe_2Ta and Fe_2W.

Due to the complicated electronic structure, which was illustrated in Figs. 2(g) and 3(g), it is difficult to predict the effect of alloying on properties such as the MAE without explicitly doing calculations to evaluate the properties. For the system studied here it is also of interest to investigate where the transition from ferro- to ferrimagnetism occurs. The virtual crystal approximation [34] (VCA), in which the alloyed atoms are exchanged for virtual atoms with noninteger effective atomic numbers, Z, which on average have the right ionic charge and number of electrons for a given alloy concentration, will be used to treat the disorder. The VCA, although simple compared to more sophisticated single site approximations, such as the coherent potential approximation (CPA), often provides a good average description for properties such as magnetic moments [3,35–37], especially for neighbors in the periodic table and small alloy concentrations [34]. For delicate properties, like the MAE, on the other hand, the VCA has often been seen to result in quantitative discrepancies compared to CPA calculations [37,38], supercell calculations [39,40], or experiments [37,41,42]. Nevertheless, one should still be able to observe correct qualitative trends in the MAE from the VCA and it will be applied also for this property. Additionally, the discrepancies in the MAE observed when comparing the VCA with more sophisticated methods, mentioned above, were found in cases where magnetic elements, such as Fe and Co, were alloyed with each other. Here, alloying is considered between the nonmagnetic constituents Ta and W, whereby one might expect better performance from the VCA when studying magnetic properties.

Calculations were performed for values of x in increments of 0.1. A calculation for $x = 0.1$ revealed that this is enough for the magnetic ordering to transition into the ferrimagnetic ordering observed also for Fe_2W. A complete structural relaxation, using spin polarized calculations neglecting SOC, was thus performed for $x = 0.1$. The resulting lattice parameters are $a = 4.771$ Å and $c = 7.847$ Å. Lattice parameters for $0.2 \leqslant x \leqslant 0.9$ were calculated by linear interpolation between the values obtained for $x = 0.1$ and $x = 1.0$. Calculations including SOC were then performed for the whole range of alloys and the resulting spin magnetic moments (for magnetization along the c axis) and MAEs are presented in Fig. 6. A large decrease in total spin magnetic moment is seen when going from $x = 0$ to $x = 0.1$, due to the change in sign of the Fe_1 spin moment, but also because of an accompanying reduction in size of the Fe_2 moment. For x greater than 0.1, the total spin magnetic moment monotonically increases until $x = 1.0$. This appears to be from a combination of a decrease in size of the Fe_1 moment and an increase in size of the Fe_2 moment. The MAE decreases with x until it reaches a minimum at $x = 0.5$ and then increases until $x = 1.0$. Hence, the largest positive values of the MAE are obtained for the end compounds and it cannot be increased by the alloying considered here. A negative in-plane anisotropy of very large magnitude is seen for $x = 0.5$. However, it is important to remember that the VCA has often been seen to overestimate the magnitude of the MAE, whereby the real value might be of smaller magnitude.

Due to limitations in the VCA, it is desirable to compare the MAE calculations with a more realistic model of disorder, such as supercell calculations. Unfortunately, a realistic description of a delicate property, such as the MAE, is computationally very demanding. Not only must one use large supercells with broken symmetry in combination with accurate Brillouinzone integration, but averaging over several of these supercells is necessary [40,43]. Even if using so-called special quasirandom structures [44], such an averaging is necessary for an adequate description of the MAE [45]. Thus, a complete study using such methods becomes prohibitively expensive and is beyond the scope of the current work. Nevertheless, to obtain a comparison with the VCA results, the case of $x = 0.25$ has

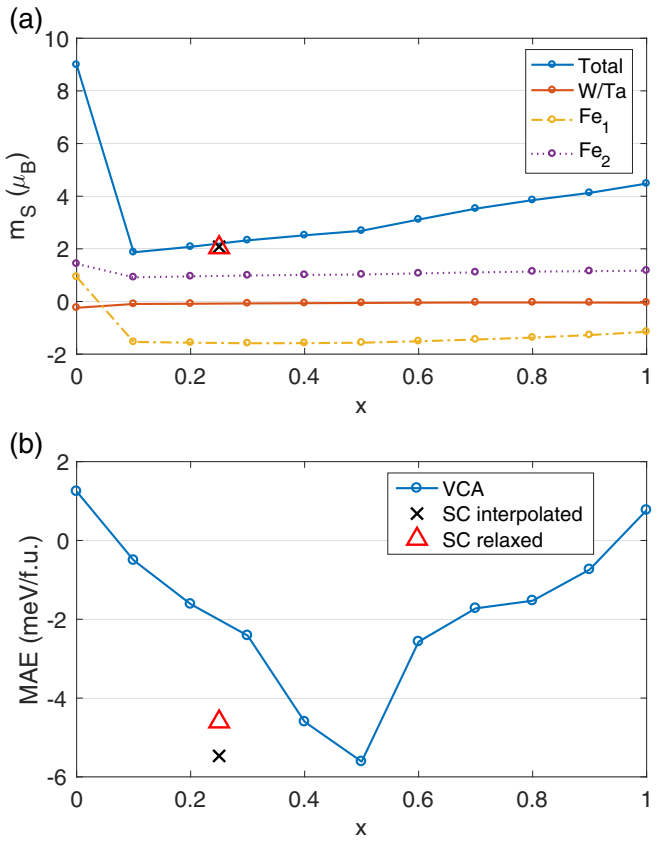

FIG. 6. (a) Spin magnetic moments and (b) MAE (computed as total-energy differences for magnetizations along 100 and 001 directions) as functions of x in $Fe_2Ta_{1-x}W_x$.

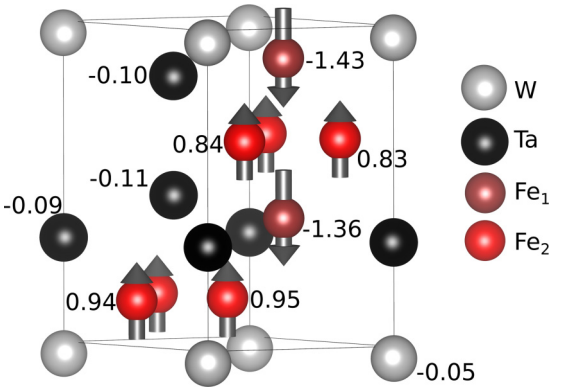

FIG. 7. Structure with three Ta atoms and one W atom. Numbers indicate the magnetic moments on the atoms in units of Bohr magnetons.

been studied by replacing one of the four equivalent Ta atoms in a unit cell by a W atom. Calculations were first performed using the structural parameters obtained by linear interpolation between those of $x = 0.1$ and $x = 1.0$, and then by optimizing the lattice parameters and relaxing the internal atomic positions for the supercell. The structural optimization resulted in a slightly smaller lattice parameter of $a = 4.728$ Å and $c = 7.785$ Å, compared to the interpolated values of $a = 4.755$ Å and $c = 7.834$ Å. The computed magnetic moments and MAEs are included in Fig. 6. The magnetic moments of Fe_1 and Fe_2 are antiparallel in agreement with the VCA calculations. The total magnetic moment is nearly identical for the two supercell calculations and both values agree well with that from the VCA calculation, as expected. Direct comparison of individual moments is complicated by the symmetry breaking in the supercell which results in a larger number of different magnetic moments. The individual magnetic moments tend to be slightly larger for the interpolated structure than the relaxed structure, consistent with the somewhat larger unit-cell volume, which tends to allow larger magnetic moments to form. However, cancellation between the negative magnetic moments on Fe_1 sites and positive magnetic moments on Fe_2 sites results in merely a small difference of $0.03\mu_B$ in the total magnetic moment per unit cell. The magnetic moments in units of Bohr magnetons for each atom in the unit cell of the relaxed structure are shown in Fig. 7. The small variations in magnetic moments between different Fe_1 sites, different Fe_2 sites, or different Ta and the W sites is an effect beyond what can be described within the single-site approximations, such as the VCA or CPA. From the data in Fig. 7, one can observe that magnetic moments on Fe atoms near W tend to be larger than those on Fe atoms near Ta.

Regarding the MAE, the values obtained for the relaxed and interpolated structures are -4.6 meV/u.c. and -5.5 meV/u.c., respectively. That is significantly larger in magnitude than the value of approximately -2 meV/u.c. expected from the VCA according to Fig. 6. Nevertheless, the VCA and supercell calculations agree in the sign change of the MAE in going from $x = 0$ to $x = 0.25$. From the currently available data it is not possible to say how much of the discrepancy is due to insufficiency of the VCA and how much is due to considering only one supercell of limited size.

V. CONCLUSIONS

A comprehensive computational study has been performed for the hexagonal Laves phase compounds Fe_2Ta and Fe_2W, with focus on the important intrinsic magnetic properties saturation magnetization and MAE. For Fe_2W, a ferrimagnetic ground state has been suggested, different from that found in earlier computational work [14]. In the case of Fe_2Ta, a similar magnetic ordering is found as in preceding calculations [14], but an opposite sign is found in the MAE. The discrepancies in comparison with earlier calculations calls for further experimental efforts to unambiguously determine the magnetic properties of these compounds.

The MAE has been carefully analyzed in terms of the electronic structure and by using the magnetic force theorem to compute **k**-point resolved contributions to the MAE. Because the density of states at the Fermi energy is dominated by $3d$ states, $5d$ states can only contribute notably to the MAE in small regions of the Brillouin zone. Nevertheless, it is found that the MAE originates mainly from regions in the Brillouin zone where there is a strong $3d$-$5d$ hybridization, allowing the strong SOC of the $5d$ atoms to increase the MAE.

The main motivation to study uniaxial $3d$-$5d$ compounds is the possibility to have a very large MAE, such as the value of

6.6 MJ/m^3 [4] observed in FePt. When a significant amount of magnetic 3*d* elements is included, this can be combined with large saturation magnetization and a high Curie temperature. Among the compounds studied here, the MAEs calculated are modest compared to that of FePt. In addition, for Fe_2W, a ferrimagnetic ordering is found, resulting in a low saturation magnetization. Nevertheless, whether a material is useful for a given application depends on a combination of the mentioned intrinsic parameters. For example, in the context of permanent magnets, the hardness parameter

$$\kappa = \sqrt{\frac{K}{\mu_0 M^2}}, \tag{6}$$

with MAE K and saturation magnetization M, can be used to determine whether a material has the potential to exhibit a reasonable coercive field and be used as a permanent magnet [4,5]. κ is required to be greater than unity but the microstructural engineering to obtain the desired properties of a permanent magnet should be easier with larger κ and Hirosawa [5] suggested $\kappa > 1.4$ to be demanded from potential permanent magnet materials. For the materials studied here one finds $\kappa = 1.8$ for Fe_2Ta and $\kappa = 2.9$ for Fe_2W, from the data in Table II, well above the requirement put forward by Hirosawa. These large values of κ appear largely because of the modest saturation magnetizations and the energy product of a permanent magnet will be limited by this. In both materials the saturation magnetization is below the value of $\mu_0 M_s = 1.6$ T [4] found in the powerful $Nd_2Fe_{14}B$ magnet. However, at least in Fe_2Ta the saturation magnetization is greater than 0.48 T seen in $BaFe_{12}O_{19}$ ferrite magnets, potentially making the compound technologically interesting as an intermediate alternative between rare-earth and ferrite magnets.

Experimental work has reported a Curie temperature of 550 K in Fe_2W [15], which should be sufficient for many technological applications. As a useful extension of the current work, it would be interesting to compute the Curie temperatures of Fe_2W and Fe_2Ta, e.g., by calculating the Heisenberg exchange parameters from first principles and using these as input to the mean-field approximation or Monte Carlo simulations. This would reveal whether Fe_2Ta also has a high enough Curie temperature to be technologically interesting and might also shed further light on the issue regarding the magnetic ordering of Fe_2W.

To investigate the possibility of enhancing the relevant properties, alloying of W and Ta has been considered in calculations for $Fe_2Ta_{1-x}W_x$, with the disorder treated in the virtual crystal approximation. These calculations indicate that the transition from ferro- to ferrimagnetic ordering occurs for x smaller than 0.1 and that the MAE is significantly reduced and mainly strongly negative in the alloy. For technological purposes this does not appear promising. However, there are various isostructural 3*d*-5*d* compounds, such as Mn_2Ta, Co_2Ta, or Fe_2Hf [17,46], and one might also consider alloys among these. Allowing for 3*d* or 4*d* atoms to substitute the 5*d* atom gives further possibilities [46]. As a next step, it should be worthwhile to investigate ternary or quaternary phase diagrams for magnetic 3*d* elements combined with 5*d* and other elements in uniaxial crystals. Numerous such phases which have not been properly characterized in terms of magnetic properties should exist and the type of computational methods used in this work should be of great value in identifying interesting materials.

TABLE IV. Matrix elements $\langle \sigma_i, d_i | \hat{\mathbf{l}} \cdot \hat{\mathbf{s}} | \sigma_j, d_j \rangle$ of the spin-orbit coupling operator with respect to spin states in direction $\hat{\mathbf{n}} = (\sin\theta\cos\phi, \sin\theta\sin\phi, \cos\theta)$ and *d* orbitals, in units of $\hbar^2$. Reproduced from Ref. [47].

	$\lvert\uparrow, d_{xy}\rangle$	$\lvert\uparrow, d_{yz}\rangle$	$\lvert\uparrow, d_{z^2}\rangle$	$\lvert\uparrow, d_{xz}\rangle$	$\lvert\uparrow, d_{x^2-y^2}\rangle$
$\langle\uparrow, d_{xy}\rvert$	0	$\frac{1}{2}i\sin\theta\sin\phi$	0	$-\frac{1}{2}i\sin\theta\cos\phi$	$i\cos\theta$
$\langle\uparrow, d_{yz}\rvert$	$-\frac{1}{2}i\sin\theta\sin\phi$	0	$-\frac{\sqrt{3}}{2}i\sin\theta\cos\phi$	$\frac{i}{2}\cos\theta$	$\frac{-i}{2}\sin\theta\cos\phi$
$\langle\uparrow, d_{z^2}\rvert$	0	$\frac{\sqrt{3}}{2}i\sin\theta\cos\phi$	0	$-\frac{\sqrt{3}}{2}i\sin\theta\sin\phi$	0
$\langle\uparrow, d_{xz}\rvert$	$\frac{1}{2}i\sin\theta\cos\phi$	$-\frac{i}{2}\cos\theta$	$\frac{\sqrt{3}}{2}i\sin\theta\sin\phi$	0	$-\frac{1}{2}i\sin\theta\sin\phi$
$\langle\uparrow, d_{x^2-y^2}\rvert$	$-i\cos\theta$	$\frac{-i}{2}\sin\theta\cos\phi$	0	$\frac{1}{2}i\sin\theta\sin\phi$	0
$\langle\downarrow, d_{xy}\rvert$	0	$-\frac{1}{2}(\cos\phi - i\cos\theta\sin\phi)$	0	$-\frac{1}{2}(\sin\phi + i\cos\theta\cos\phi)$	$-i\sin\theta$
$\langle\downarrow, d_{yz}\rvert$	$\frac{1}{2}(\cos\phi - i\cos\theta\sin\phi)$	0	$-\frac{\sqrt{3}}{2}(\sin\phi + i\cos\theta\cos\phi)$	$-\frac{i}{2}\sin\theta$	$-\frac{1}{2}(\sin\phi + i\cos\theta\cos\phi)$
$\langle\downarrow, d_{z^2}\rvert$	0	$\frac{\sqrt{3}}{2}(\sin\phi + i\cos\theta\cos\phi)$	0	$\frac{\sqrt{3}}{2}(\cos\phi - i\cos\theta\sin\phi)$	0
$\langle\downarrow, d_{xz}\rvert$	$\frac{1}{2}(\sin\phi + i\cos\theta\cos\phi)$	$\frac{i}{2}\sin\theta$	$-\frac{\sqrt{3}}{2}(\cos\phi - i\cos\theta\sin\phi)$	0	$\frac{1}{2}(\cos\phi - i\cos\theta\sin\phi)$
$\langle\downarrow, d_{x^2-y^2}\rvert$	$i\sin\theta$	$-\frac{1}{2}(\sin\phi + i\cos\theta\cos\phi)$	0	$-\frac{1}{2}(\cos\phi - i\cos\theta\sin\phi)$	0

ACKNOWLEDGMENTS

I would like to thank Y. Kvashnin for critically reading and providing useful comments on the manuscript. I am also grateful to J. Rusz and O. Eriksson for discussions and for encouragement to pursue this work. Computational work has been performed with resources from the Swedish National Infrastructure for Computing (SNIC) at the National Supercomputer Centre (NSC) in Linköping and C3SE in Gothenburg.

APPENDIX: MATRIX ELEMENTS OF THE SPIN-ORBIT OPERATOR

If $|i\rangle$ is a single-particle eigenstate to an unperturbed Hamiltonian with no SOC, the total shift in the energy E_i due to $H_{\mathrm{SOC}} = \xi \hat{\mathbf{l}} \cdot \hat{\mathbf{s}}$ in second-order perturbation theory is

$$\Delta E_i = -\xi^2 \sum_{j \neq i} \frac{|\langle n|\hat{\mathbf{l}} \cdot \hat{\mathbf{s}}|k\rangle|^2}{E_j - E_i}. \tag{A1}$$

If the unperturbed Hamiltonian commutes with the spin operator, $|i\rangle$ has a well defined spin σ_i but can be considered a superposition of different orbitals μ so in the simplest case (ignoring other quantum numbers, e.g., $\mathbf{k}$)

$$|i\rangle = \sum_{\mu} c_{i,\mu} \, |\mu,\sigma_i\rangle \, . \tag{A2}$$

For d-electron magnetism, which is of focus here, it is suitable to consider μ as d_{z^2}, d_{xz}, d_{yz}, d_{xy} or $d_{x^2-y^2}$. The numerator in Eq. (A1) then contains matrix elements $\langle d_i,\sigma_i|\,\mathbf{l}\cdot\mathbf{s}\,|\mathrm{d}_j,\sigma_j\rangle$, which determine the effect of the SOC. For convenience these matrix elements are explicitly listed in Table IV, with θ and ϕ denoting the polar and azimuthal angles of the spin quantization axis relative to the crystal lattice.

As mentioned in the main text, only coupling between states $|i\rangle$ and $|j\rangle$ with energies E_i and E_j such that $E_i < E_{\mathrm{F}} < E_j$ will contribute to the MAE and clearly then $\Delta E_i \leqslant 0$ according to Eq. (A1). In terms of the matrix elements in Table IV this means that any coupling containing $\cos\theta$ will lower the energy for $\theta = 0$, i.e., favoring a uniaxial magnetization (positive MAE), while $\sin\theta$ lowers the energy for $\theta = \pi/2$ which favors in-plane magnetization (negative MAE). The situation taking into account multiple atomic types and hybridization in Eq. (2) is somewhat more complicated and contains a product of matrix elements for possibly different atomic types. Nevertheless, the MAE is still determined by the matrix elements in Table IV.

[1] J. H. V. Vleck, Phys. Rev. **52**, 1178 (1937).
[2] O. Gutfleisch, M. A. Willard, E. Brück, C. H. Chen, S. G. Sankar, and J. P. Liu, Adv. Mater. **23**, 821 (2011).
[3] D. Niarchos, G. Giannopoulos, M. Gjoka, C. Sarafidis, V. Psycharis, J. Rusz, A. Edström, O. Eriksson, P. Toson, J. Fidler, E. Anagnostopoulou, U. Sanyal, F. Ott, L.-M. Lacroix, G. Viau, C. Bran, M. Vazquez, L. Reichel, L. Schultz, and S. Fähler, JOM **67**, 1318 (2015).
[4] J. M. D. Coey, IEEE Trans. Magn. **47**, 4671 (2011).
[5] S. Hirosawa, J. Magn. Soc. Jpn. **39**, 85 (2015).
[6] D. Weller, A. Moser, L. Folks, M. E. Best, W. Lee, M. F. Toney, M. Schwickert, J.-U. Thiele, and M. F. Doerner, IEEE Trans. Magn. **36**, 10 (2000).
[7] D. Kramer, Phys. Today **63**(5), 22 (2010).
[8] J. B. Staunton, S. S. Ostanin, S. S. A. Razee, B. Gyorffy, L. Szunyogh, B. Ginatempo, and E. Bruno, J. Phys.: Condens. Matter **16**, S5623 (2004).
[9] J. B. Staunton, S. Ostanin, S. S. A. Razee, B. L. Gyorffy, L. Szunyogh, B. Ginatempo, and E. Bruno, Phys. Rev. Lett. **93**, 257204 (2004).
[10] S. Okamoto, N. Kikuchi, O. Kitakami, T. Miyazaki, Y. Shimada, and K. Fukamichi, Phys. Rev. B **66**, 024413 (2002).
[11] T. Burkert, O. Eriksson, S. I. Simak, A. V. Ruban, B. Sanyal, L. Nordström, and J. M. Wills, Phys. Rev. B **71**, 134411 (2005).
[12] J. Lyubina, I. Opahle, K.-H. Müller, O. Gutfleisch, M. Richter, M. Wolf, and L. Schultz, J. Phys.: Condens. Matter **17**, 4157 (2005).
[13] H. Arnfelt and A. Westgren, Jernkontorets Ann. **119**, 185 (1935).
[14] P. Kumar, A. Kashyap, B. Balamurugan, J. E. Shield, D. J. Sellmyer, and R. Skomski, J. Phys.: Condens. Matter **26**, 064209 (2014).
[15] M. A. Koten, P. Manchanda, B. Balamurugan, R. Skomski, D. J. Sellmyer, and J. E. Shield, APL Mater. **3**, 076101 (2015).
[16] S. Ishida, S. Asano, and J. Ishida, J. Phys. Soc. Jpn. **54**, 4695 (1985).
[17] Ž. Blažina and S. Pavković, J. Less-Common Met. **155**, 247 (1989).
[18] J. P. Perdew, K. Burke, and M. Ernzerhof, Phys. Rev. Lett. **77**, 3865 (1996).
[19] P. Blaha, G. Madsen, K. Schwarz, D. Kvasnicka, and J. Luitz, *WIEN2k, An Augmented Plane Wave + Local Orbitals Program for Calculating Crystal Properties* (Karlheinz Schwarz, Techn. Universität Wien, Austria, 2001).
[20] D. D. Koelling and H. N. Harmon, J. Phys. C **10**, 3107 (1977).
[21] P. E. Blöchl, O. Jepsen, and O. K. Andersen, Phys. Rev. B **49**, 16223 (1994).
[22] A. I. Liechtenstein, M. I. Katsnelson, V. P. Antropov, and V. A. Gubanov, J. Magn. Magn. Mater. **54-57**, 965 (1986).
[23] R. Wienke, G. Schütz, and H. Ebert, J. Appl. Phys. **69**, 6147 (1991).
[24] A. Edström, J. Chico, A. Jakobsson, A. Bergman, and J. Rusz, Phys. Rev. B **90**, 014402 (2014).
[25] J.-U. Thiele, L. Folks, M. F. Toney, and D. K. Weller, J. Appl. Phys. **84**, 5686 (1998).
[26] P. Ravindran, A. Kjekshus, H. Fjellvaag, P. James, L. Nordström, B. Johansson, and O. Eriksson, Phys. Rev. B **63**, 144409 (2001).
[27] E. I. Kondorskii and E. Straube, Zh. Eksp. Teor. Fiz. **63**, 356 (1973) [Sov. Phys. JETP **36**, 188 (1973)].
[28] P. Bruno, Phys. Rev. B **39**, 865 (1989).
[29] C. Andersson, B. Sanyal, O. Eriksson, L. Nordström, O. Karis, D. Arvanitis, T. Konishi, E. Holub-Krappe, and J. H. Dunn, Phys. Rev. Lett. **99**, 177207 (2007).

[30] D.-S. Wang, R. Wu, and A. J. Freeman, Phys. Rev. B **47**, 14932 (1993).
[31] A. Edström, Ph.D. thesis, Uppsala Universitet, 2016.
[32] G. H. O. Daalderop, P. J. Kelly, and M. F. H. Schuurmans, Phys. Rev. B **41**, 11919 (1990).
[33] G. H. Lander, M. S. S. Brooks, B. Lebech, P. J. Brown, O. Vogt, and K. Mattenberger, Appl. Phys. Lett. **57**, 989 (1990).
[34] J. Faulkner, Prog. Mater. Sci. **27**, 1 (1982).
[35] R. H. Victora and L. M. Falicov, Phys. Rev. B **30**, 259 (1984).
[36] E. K. Delczeg-Czirjak, A. Edström, M. Werwinski, J. Rusz, N. V. Skorodumova, L. Vitos, and O. Eriksson, Phys. Rev. B **89**, 144403 (2014).
[37] A. Edström, M. Werwiński, D. Iuşan, J. Rusz, O. Eriksson, K. P. Skokov, I. A. Radulov, S. Ener, M. D. Kuz'min, J. Hong, M. Fries, D. Y. Karpenkov, O. Gutfleisch, P. Toson, and J. Fidler, Phys. Rev. B **92**, 174413 (2015).
[38] I. Turek, J. Kudrnovský, and K. Carva, Phys. Rev. B **86**, 174430 (2012).
[39] C. Neise, S. Schönecker, M. Richter, K. Koepernik, and H. Eschrig, Phys. Status Solidi B **248**, 2398 (2011).
[40] S. Steiner, S. Khmelevskyi, M. Marsmann, and G. Kresse, Phys. Rev. B **93**, 224425 (2016).
[41] G. Andersson, T. Burkert, P. Warnicke, M. Björck, B. Sanyal, C. Chacon, C. Zlotea, L. Nordström, P. Nordblad, and O. Eriksson, Phys. Rev. Lett. **96**, 037205 (2006).
[42] L. Reichel, G. Giannopoulos, S. Kauffmann-Weiss, M. Hoffmann, D. Pohl, A. Edström, S. Oswald, D. Niarchos, J. Rusz, L. Schultz, and S. Fähler, J. Appl. Phys. **116**, 213901 (2014).
[43] M. Däne, S. K. Kim, M. P. Surh, D. Aberg, and L. X. Benedict, J. Phys.: Condens. Matter **27**, 266002 (2015).
[44] A. Zunger, S.-H. Wei, L. G. Ferreira, and J. E. Bernard, Phys. Rev. Lett. **65**, 353 (1990).
[45] M. Werwiński (private communication).
[46] Y. Nishihara, J. Magn. Magn. Mater. **70**, 75 (1987).
[47] E. Abate and M. Asdente, Phys. Rev. **140**, A1303 (1965).